Increasing perpendicular alignment in extruded filament by an orifice embedded 3D printing nozzle

Do-In Jeong, Ankur Jain & Dong-Wook Oh

Published online: 04 Oct 2021.

Submit your article to this journal ↗

Article views: 82

View related articles ↗

View Crossmark data ↗

Taylor & Francis
Taylor & Francis Group

Check for updates

Increasing perpendicular alignment in extruded filament by an orifice embedded 3D printing nozzle

Do-In Jeong[a], Ankur Jain [b] and Dong-Wook Oh [a]

aDepartment of Mechanical Engineering, Chosun University, Gwangju, Korea; bMechanical and Aerospace Engineering Department, University of Texas at Arlington, Arlington, TX, USA

ABSTRACT

The mixing of fibrous additives in the polymer base is being widely investigated for improving the mechanical properties of printed parts using fused filament fabrication (FFF). In this study, flow visualisation experiments and computational fluid dynamics (CFD) analysis were conducted on the flow channel of a nozzle with an orifice for enhancing the through-layer physical properties of the printed parts. Flow visualisation experiments were conducted on the flow channels of nozzles installed with orifices of various shapes. Using ball-milled carbon fibre in high-viscosity polydimethylsiloxane (PDMS) that imitates filament flow in FFF, the fibre angles were measured for different internal and external locations of the nozzle. The distribution of the fibre angles inside the nozzle was compared with the gradient of the flow field calculated for the same shape by CFD analysis. It was found that the orifice structure inside the nozzle increases the vertical alignment of the fibre. An abrupt increase in the extension rate at the exit of the orifice is considered to be the reason behind the rotation and vertical orientation of fibres inside the nozzle channel. Results presented in this work provide the basis for achieving improved through-plane physical properties of FFF printed parts through fibre alignment.

1. Introduction

Polymer additive manufacturing techniques such as fused filament fabrication (FFF) (El Moumen, Tarfaoui, and Lafdi 2019; Yuan et al. 2019; Goh and Yeong 2018) rely on deposition of thin polymer filaments that are heated to above the glass transition temperature. However, incomplete adhesion between adjacent filaments often results in parts with poor mechanical properties. The addition of a small fraction of an additive to the base polymer has been widely investigated for improving the properties of printed parts, such as corrosion resistance (Kausar 2019), electrical properties (Castles et al. 2016), mechanical properties (Caminero et al. 2018; Ning et al. 2015; Young, Wetmore, and Czabaj 2018; Waheed et al. 2019; Hwang et al. 2014) and thermal conductivity (Waheed et al. 2019; Hwang et al. 2014; Nikzad, Masood, and Sbarski 2011). Commonly used additives include ceramics (Castles et al. 2016), carbon (Caminero et al. 2018; Ning et al. 2015) and metal (Hwang et al. 2014; Nikzad, Masood, and Sbarski 2011) in a variety of forms such as nanoparticles, microparticles and fibres, and over a broad size range from a few nm to tens of μm (Kausar 2019; Castles et al. 2016; Caminero et al. 2018; Ning et al. 2015; Young, Wetmore, and Czabaj 2018; Waheed et al. 2019;

Hwang et al. 2014; Nikzad, Masood, and Sbarski 2011; Mohan et al. 2017). Research has been reported on understanding the fundamental mechanisms underlying the measured property improvements (Hwang et al. 2014). Increments of 30% in tensile strength and 430% in thermal conductivity of acrylonitrile butadiene styrene (ABS) mixed with 7.5% wt. of carbon fibre and 40% wt. of copper nanoparticle, respectively, were reported (Young, Wetmore, and Czabaj 2018; Nikzad, Masood, and Sbarski 2011). In general, such properties are found to improve proportionally with the fraction of the additive material. For example, adding micro-sized diamond particles to polylactic acid (PLA) base in weight fractions of 10%, 30% and 50% was found to increase the thermal conductivity of composites by 24%, 207% and 424%, respectively, compared to pristine PLA (Su et al. 2018). However, adding very high concentration of additives is not desirable, due to adverse effects such as an exponential increase in the viscosity of the melted mixture, an increase in the pressure needed to dispense the filament and a reduction in the plasticity of the finished products (Nikzad, Masood, and Sbarski 2011).

In light of these trade-offs, it is important to carefully design the composite material in order to achieve the

best possible improvement in physical properties within a realistic concentration that does not disrupt the 3D printing process (Nikzad, Masood, and Sbarski 2011; Berretta et al. 2017). Specifically, in the context of one- or two-dimensional additives such as carbon fibres or graphene materials, understanding and controlling the alignment of the fibres is critical (Chen, Wu, and Jiang 2019; Su, Wu, and Jiang 2012; Goh, Agarwala, and Yeong 2019). It is generally known that physical properties such as mechanical strength and thermal conductivity of a polymer composite are significantly improved in the fibre alignment direction, with much lower improvement in the direction normal to the alignment direction (Gong, Zhu, and Meguid 2015; Holmes and Riddick 2014; Kokkinis, Schaffner, and Studart 2015; Yan et al. 2014; Yuan et al. 2015; Mulholland et al. 2018; Consul et al. 2021; Yeong and Goh 2020). Furthermore, owing to factors such as air gap and voids between adjacent layers, physical properties in the through-layer direction may even be worse than those of the raw material (Prajapati et al. 2018). Consequently, there is a need for developing techniques that may be used for improving through-layer fibre orientation and, therefore, physical properties of printed parts.

Motivated by the reasons discussed above, numerous studies have been reported for analysing the process behind fibre alignment during FFF and thus improving the physical properties of printed parts. Anwer and Naguib (2018) compared the physical properties and the surface characteristics of FFF products with different alignment angles of multiwalled carbon nanotubes in the filament polymer. Lewicki (2018) proposed making the fibre alignment more parallel to the raster direction by inserting microchannel-structured flow channels inside the extruding nozzle. Tekinalp et al. (2014) compared the anisotropy of samples manufactured by compression moulding (CM) and FFF. Their research results showed that the additives are aligned more in the printing direction in FFF parts than in CM parts. Studies to magnetically activate the fibre alignment process have also been reported. Shulga et al. (2020) utilised X-ray micro-computed tomography (micro-CT) to characterise the printed parts in three dimensions and correlate with mechanical strength. Nagarajan et al. (2018) demonstrated that fibre alignment in printed parts can be controlled by magnetic field generated by a neodymium magnet by mixing PR-48 resin with strontium ferrite. In principle, particle imaging velocimetry (PIV) can also be used for the visualisation of fibre alignment within an FFF polymer matrix; however, there appears to be lack of work in this direction. In recent studies, fibre alignment inside the extruded filaments was found to change due to

squeeze flow between the nozzle and the bed or already deposited layer (Heller, Smith, and Jack 2019; Wang and Smith 2021). The gap distance between the nozzle and the bed and the shape of free surface of the bead at the nozzle exit were found to affect the alignment of fibres inside the deposition and the resulting bulk mechanical properties through a numerical analysis and experiments (Consul et al. 2021).

In the aforementioned studies cross-sectional visualisation of a printed part has been commonly carried out using optical methods for fibre alignment analysis. However, it is difficult to perform fibre alignment analysis using a destructive method after printing to reveal the correlation between the flow field in the liquifier and the additive rotation. Moreover, there is a lack of studies that control the fibre alignment in the through-layer direction, except the aforementioned work by Nagarajan et al. (2018). Alignment of a fibrous additive in a direction vertical to the flow direction has been commonly achieved in the traditional moulding process by using a mould containing an orifice (Nguyen and Oh 2020; Trebbin et al. 2013; Pathanasiou and Guell 1997; Butler 1999). However, there is insufficient past work on the quantitative effects of orifice thickness and flow speed on vertical fibre alignment in the context of additive manufacturing. To overcome the limitations of the existing literature, this study carries out experimental measurements and numerical simulations of the fibre alignment process within a polymer matrix, with the goal of improved fibre alignment in additive manufacturing of composite polymers. If it is possible to derive an FFF nozzle that can control the alignment of additives in a specific direction, it will be possible to fabricate products for multi-functional structures and 3D electronics (Gardner et al. 2016; Guo et al. 2015; Goh et al. 2021) that has higher electrical and mechanical physical properties at even with a small concentration of additives.

In this study, fibre alignment inside filaments extruded with various extrusion speeds in a nozzle with an orifice channel was observed using the flow visualisation method. Flow visualisation experiments were conducted inside the mould flow channel using 7 μm diameter and 88 μm long carbon fibres in a transparent polymer that is rheologically similar to commonly used FFF polymers that are opaque and, therefore, inappropriate for flow visualisation. A mixture of carbon fibre and uncured polydimethylsiloxane (PDMS) was extruded into a transparent flow channel that mimics an FFF nozzle. Fibre alignment in the polymer prior to extrusion and in the deposited raster after extrusion was observed. The impact of orifice shape on the change in fibre alignment angle in the through-layer direction was analysed. Furthermore, the results were

compared with the general nozzle results obtained with an internal flow channel having a constant diameter. Experimental measurements were compared with a computational fluid dynamics (CFD) simulation. It was found that the orifice structure inside the nozzle increases the vertical alignment of fibres and can be used to enhance through-plane physical properties of the printed part.

2. Methods

2.1. Experiment design

To optimally design the experiments for observing the fibre alignment occurring during the FFF process of the polymer composite and dependence of fibre alignment on the orifice shape inside the nozzle, the scope of experimental observation and working fluid selection issues were first considered. In a general FFF process, the fibre alignment is set inside the nozzle flow channel before being extruded from the nozzle and is typically parallel to the raster direction (Shofner et al. 2003), as presented in Figure 1(a). The key objective of this study was to contribute towards improving the through-layer physical properties of the polymer composite manufactured using the FFF method. For this purpose, fibre alignment vertical to the raster direction was increased by installing an orifice structure inside the extrusion nozzle.

The main observation target in the flow visualisation experiments was the inner flow channel of the extrusion nozzle. As mentioned above, fibre alignment during the FFF process is expected to be mostly set inside the nozzle flow. First, the additive inside the nozzle rotates under the effect of the shear stress, which rapidly changes because of several factors, such as the orifice structure, no-slip conditions of the nozzle wall, flow speed and viscosity of the liquified polymer composite mixture. However, after being extruded from the nozzle, the shear stress at the interface between the extruded filament and air becomes close to zero. Consequently, the shear stress in the extruded filament and the additive alignment do not change after the nozzle exit, except when it bends to 90° because of contact with the bed or an already deposited layer. This phenomenon was experimentally verified, and thus, the extrusion nozzle and the filament immediately after being extruded from the nozzle were selected as the observation targets in the experiments.

To supplement experimental observations of the correlation between fibre alignment and the flow field, flow in a channel configuration representative of the nozzle used in the experiments was calculated by CFD analysis. In the CFD analysis, the liquified polymer composite was assumed to be a single-phase fluid. Moreover, the flow fields in the channel inside the nozzle and filament outside the nozzle were analysed and compared with the additive angle change obtained by the flow visualisation experiments. We investigated the correlation between the statistical fibre alignment angle and the shear and extension rates, which are the gradient components of the filament flow direction speed (v) and the speed vertical to the flow direction (u), respectively, in the flow field in the filament calculated by CFD. The plot of the shear and extension rates inside the filament during the FFF process is presented in Figure 1(b).
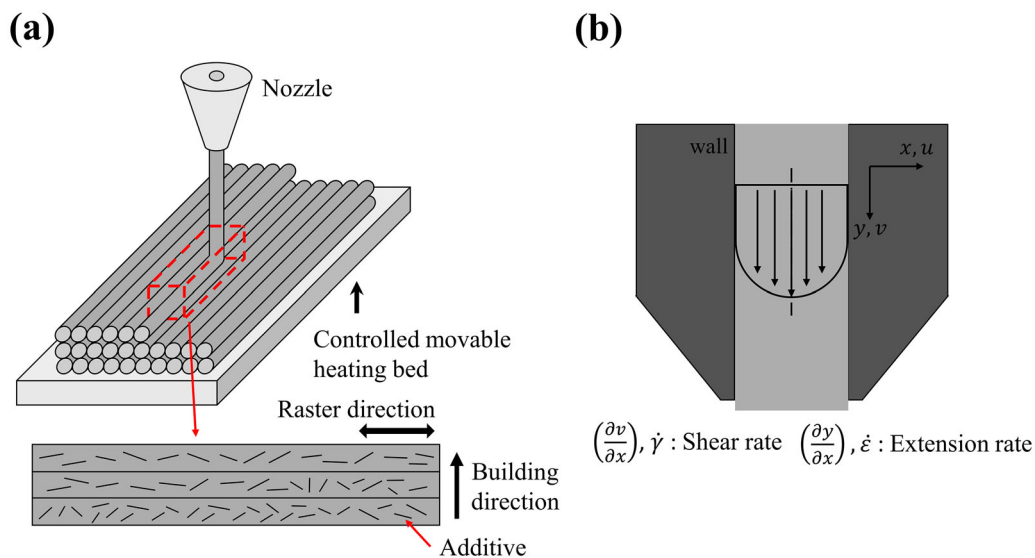

$$\left(\frac{\partial v}{\partial x}\right), \dot{\gamma} : \text{Shear rate} \quad \left(\frac{\partial y}{\partial x}\right), \dot{\varepsilon} : \text{Extension rate}$$

Figure 1. Schematic of extruding process of polymer composite with fibre-type additive in FFF: (a) overall process and (b) flow field inside the nozzle.

PDMS (Sylgard 186, Dow Co.), containing a highly viscous base and a curing agent, mixed with 7 μm diameter and 88 μm long carbon fibres was selected as the working fluid to mimic the polymer composite in FFF. PDMS has been widely used as a printing material for direct ink writing (Lewis 2006), but with limited applications in other 3D printing techniques (Ozbolat et al. 2018). Also, PDMS is an ideal polymer for the flow visualisation due to its transparency and suffices the objective of the present work. Specifically, for the extrusion process, which is the main objective of this study, the transparent nature of liquified PDMS enables visual observation of the inside of the liquified polymer material that is not possible with more common FFF materials such as acrylic that are opaque. The PDMS polymer utilised in this study has a viscosity of 66.7 Pa·s (Sylgard 186 Silicone Elastomer Technical Data Sheet, Dow Co.), which is 20 times higher than that of general-purpose PDMS (Dow Co., Sylgard 184) commonly used for soft-lithography. In spite of using the transparent PDMS with the highest viscosity, when compared to typical thermoplastic polymers for FFF, the viscosity of polymer melts is typically an order of magnitude larger. Further discussion regarding the effect of viscosity of the working fluid on the fibre alignment is covered in Section 3. Nevertheless, we believe a flow condition similar to an extruded filament in FFF is obtained with the use of PDMS due to the small changes in the relative value of velocity gradients of the flow field and, consequently, the lack of dependence on viscosity.

Ball-milled carbon fibres of a diameter and an average length of 7 and 88 μm, respectively, were used as additive and were mixed with liquified PDMS in a mass ratio of 0.07% (volume ratio of 0.04%). This mass ratio is lower than the generally reported additive concentration in polymer composites for 3D printing. However, as mentioned previously, this concentration was selected owing to the constraint of visually observing the additive alignment by flow visualisation. Conventionally, this concentration is a dilute phase in which the interaction between the additive particles does not affect the additive alignment (Pathanasiou and Guell 1997). The additive concentration for a polymer composite in a general FFF process exceeds 1%. It is known that in this concentration range, the additive–additive and additive–wall interactions become important. Compared with a previous research in which additives vertically aligned in an abruptly expanded flow channel were analysed, generally identical additive alignments were observed with both low and high additive concentrations of 0.07% (Nguyen and Oh 2020) and 30% (Trebbin et al. 2013), respectively. Based on these two

cases, it is inferred that the general representation and understanding of additive alignment during an actual FFF process is possible through the analysis of the additive alignment in the dilute state as performed in this study.

2.2. Experimental set-up

The experimental equipment to analyse the additive alignment during the FFF process can be divided into the flow channel of extrusion nozzle, an optical apparatus for the flow visualisation and a part related to the working fluid. The assembly of the block with the nozzle and the total experimental apparatus are shown in Figure 2. The optical equipment for the flow visualisation was composed of a high-speed camera (Phantom, MIRO C110) combined with an optical microscope (Mitutoyo, VMU-V) with a 2× objective lens (Mitutoyo, M plan APO 2×) for observing the inside of the nozzle channel. The optical assembly was placed on top of an x, y and z stage, and the focus of the microscope was fixed to 1.5mm inner plane of the front acrylic plate. A flat LED lighting pad placed at the opposite side of the high-speed camera was utilised as the light source. Using the high-speed camera, the inside of the flow channel with an installed orifice and after being extruded from the nozzle were separately recorded. The flow visualisation image recorded a 2.16×1.35 mm^2 window with a resolution of 768×480 pixels and in 60 frames per second using the high-speed camera. The lightness and brightness of the obtained flow visualisation image were adjusted by the image correction programme of the camera. The correction was conducted to sharpen the fibres that were in-focused compared to the background and out-focused fibres. The location, length and angle data of the fibres were extracted from the corrected images using the analysis particle function of the ImageJ software (National Institutes of Health, USA). A total of 20–100 flow visualisation images were analysed for each flow case, and the time interval between the images was set as over 2 s to prevent the duplication of single fibre results.

The base of Sylgard 186 and a curing agent were mixed in a ratio of 10:1 and used as the working fluid. The carbon fibres used as the additive were ball-milled and had a diameter of 7 μm. The average length of a total of 23,000 carbon fibres obtained by the flow visualisation experiments was 88 μm with a standard deviation of 24 μm. To obtain a more uniform carbon fibre length, the carbon fibre powder was sieved twice using a mesh of 60 μm in size and subsequently mixed with PDMS. The carbon fibres were mixed with PDMS
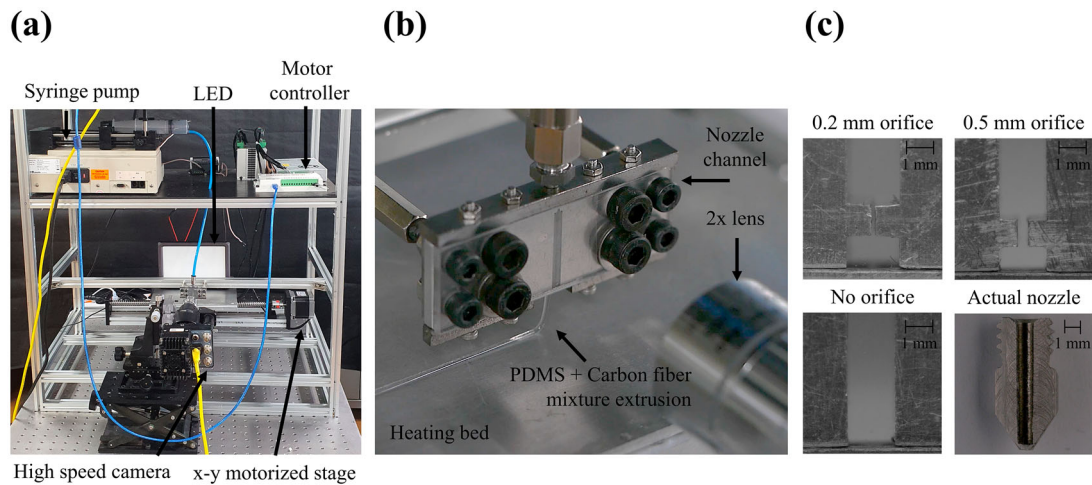
Figure 2. Experimental set-up for flow visualisation: (a) overall set-up, (b) extrusion process and (c) cross-section of nozzles.

in a mass ratio of 0.07%, which is the concentration deduced from several tests for recording sufficiently large number of fibres in a single image without overlap of the fibres in the flow visualisation image. The mixture was degassed in a centrifuge (Nasco Medilab, L450) at 4000 rpm for 3 min in order to remove air bubbles included during the hand mixing. The carbon fibres did not aggregate at the bottom of PDMS during the degassing process, and no precipitation phenomenon of the carbon fibres attributed to gravity was observed during the experiments. Additionally, fibres were well mixed inside the PDMS medium and no aggregate was observed, even inside the nozzle flow channel just up-stream of the orifice. The mixture was placed in a 50 mL syringe and pumped into the flow channel by a high-pressure syringe pump (KD Scientific Inc., KDS-410). The syringe pump and the flow channel were connected by a polyurethane tube, and the working fluid was pumped at three different flow rates of 0.1, 0.2 and 0.4 mL/min. Reynolds numbers in the nozzle channel and the speed of extruded filament corresponding to these three flow rates were 1.12×10^{-4}, 2.24×10^{-4} and 4.48×10^{-4} and 2.12, 4.25 and 8.49 mm/s, respectively. These low values indicate laminar flow in the experiments. The nozzle flow channel, flow visualisation experimental apparatus and working fluid parts were assembled together and are presented in Figure 2(a). The actual printing was extruded on the x and y motor-adjusting stages with the temperature maintained at 150 °C, while all other parts were in a room temperature of 25°C. Carbon fibre and PDMS mixture were dispensed in room temperature unlike a typical FFF process where the nozzle is maintained above the glass transition temperature of the extrusion polymer. The actual image of the PDMS and carbon fibre mixture being

extruded through the nozzle with an orifice is shown at Figure 2(b). During this process, the space between the stage and the nozzle was adjusted to be 10 mm.

Although the general FFF process nozzle is a cylindrical-shaped flow channel, in this study, orifices of various shapes were investigated, as shown in Figure 2(c). The orifice shapes were manufactured referring to the mould flow channel in a previous study (Nguyen and Oh 2020) that simulated injection moulding. Figure 3(a–c) shows the internal flow channel of the extrusion nozzle utilised in this experiment. The flow channel is composed of a total of six components. After placing a bilaterally symmetric aluminium (Al) insert for forming the orifice flow channel at the centre, the Al support and transparent acrylic visualisation windows are assembled at the top and bottom and the front and rear, respectively. The cross-section of the flow channel, excluding the orifice, is a rectangle with a width and a height of 2 and 3 mm, respectively. Furthermore, there is a circular hole with a diameter of 1 mm at the centre of the Al support with a thickness of 1 mm at the bottom of the part where the filament is discharged and extruded. Al inserts with internal orifice widths of 0.2 and 0.5 mm are presented in Figure 3(a,b), respectively. For the flow channel with no orifice, as shown in Figure 3(c), an orifice with a width of 0.5 mm was turned upside down and used. Finally, a general FFF nozzle without an orifice (diameter of 1 mm) was also tested, which is presented in Figure 3(d). The total length of the manufactured nozzle flow channel was 20 mm. For the observation of the fibre alignment inside the flow channel, a transparent acrylic plate with a thickness of 2 mm was used at the front and back sides. The total channel parts were assembled with a total of 12 bolts and nuts, forming a single block.
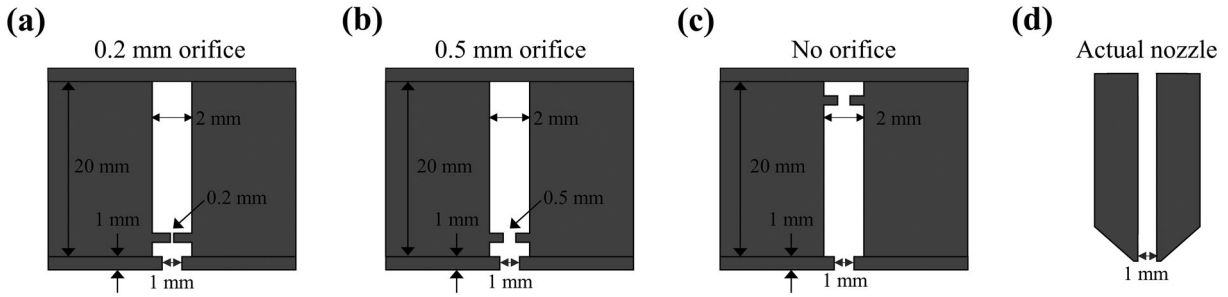
Figure 3. Schematic diagrams of the extrusion nozzle channels with various orifice thicknesses: (a) 0.2 mm orifice, (b) 0.5 mm orifice, (c) no orifice and (d) actual nozzle.

2.3. Computational fluid dynamics analysis

To correlate the carbon fibre alignment during FFF with the flow fields inside and outside the extrusion nozzle, a three-dimensional geometrical model of the flow channel used in the experiments was developed. Furthermore, computational fluid dynamics (CFD) analysis was conducted using ANSYS-Fluent (version 17.1). SIMPLE algorithm was utilised as the analysis method, and the convergence criterion for calculating the continuity equations was set as 10^{-4}. A density of a single-phase Sylgard 186 mixture of 1.12 g/cm^3 is used (Sylgard 186 Silicone Elastomer Technical Data Sheet, Dow Co.). Since the mixture shows non-Newtonian behaviour, the relationship between shear rate and viscosity was measured by using a rotational rheometer (Anton Parr, MCR 102) in the shear rate range from 0.1 s^{-1} to 200 s^{-1}. The measured result is shown in Figure 4. The experimental data are curve fitted by using the Carreau model with the following function (Kennedy and Zheng 2013):

$$\mu_{app} = \mu_\infty + (\mu_0 - \mu_\infty)[1 + (\lambda\dot{\gamma})^2]^{(n-1)/2} \qquad (1)$$

where, the fitting values of zero-shear viscosity (μ_0), time constant (λ), infinite-shear viscosity (μ_∞) and power-law index (n) of 53.6 Pa·s, 6.13 s, 0.96 Pa·s and 0.64, respectively, are found to best fit the measured data as shown in Figure 4. These viscosity parameters were provided as inputs to the simulation in order to account for the non-Newtonian behaviour of the polymer-fibre mixture.

Three different flow rates at the inlet – 0.1, 0.2 and 0.4 mL/min – were simulated, identical to experiments. Pressure at the exit was set as 0 Pa. The no-slip condition was applied at the internal wall of the nozzle flow channel, and shear stress at the walls was set as zero after the nozzle exit. Simulations were carried out on the four nozzle flow channel configurations presented in Figure 3, which is identical to the flow visualisation experiments. Analysis was performed up to 10 mm downstream of the nozzle exit. The overall geometry of

the simulation models is shown in Figure 5. The diameter of the cylinder extruded filament after the nozzle exit was determined to be 1.2 mm by flow visualisation image analysis. This value is larger than the nozzle diameter of 1 mm because of die swell of the PDMS and fibre mixture.

To verify mesh independence of the simulations, results for approximately 21, 41 and 54 million elements were compared for the nozzle flow channel with a 0.2 mm orifice. The flow direction speed, v is plotted in Figure 6 for a different number of elements. Amongst the meshes used here, v measured at a location of 0.2 mm from the orifice exit showed a difference of only 0.2%, and therefore, in this study, the mesh of 54 million elements was chosen for all further simulations.

To compare CFD results with flow visualisation experimental data, v with different orifice sizes from the nozzle exit were compared and are illustrated in Figure 7. From the two images consecutively recorded with a 0.1 s time interval in the flow visualisation experiments, the speed was obtained after calculating the change in the locations of the individual fibres from the exit of the nozzle in the extrusion direction. The experimental and CFD analysis results showed good agreement and were verified using the fibre speed obtained from the flow visualisation.

3. Result and discussion

3.1. Flow visualisation

This study aims to observe and characterise the alignment of additive particles in FFF-printed parts and understand the impact of nozzle shapes and extrusion velocities. Flow visualisation experiments using carbon fibre in PDMS polymer are used as the filament material. Figure 8 shows flow visualisation images inside the nozzle and immediately after the nozzle extrusion when the liquified mixture is injected into the nozzle at a flow rate of 0.2 mL/min. Figure 8(a) presents flow
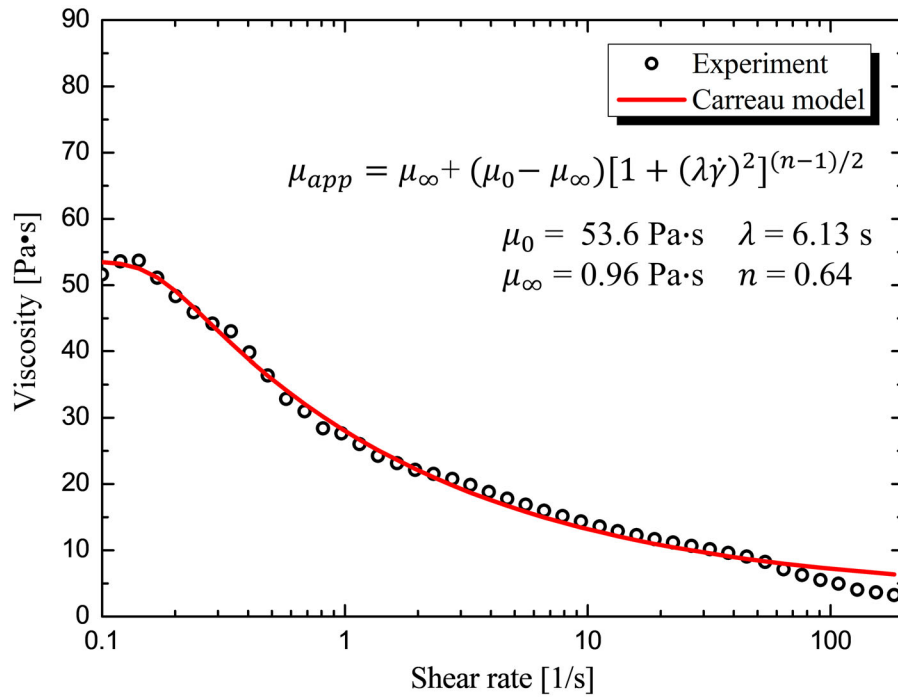
Figure 4. Measured relationship between the viscosity and shear rate of carbon fibre (0.07% wt.) and uncured PDMS mixture. Experimental results are presented as circles and solid line represents best fit by the Carreau model.
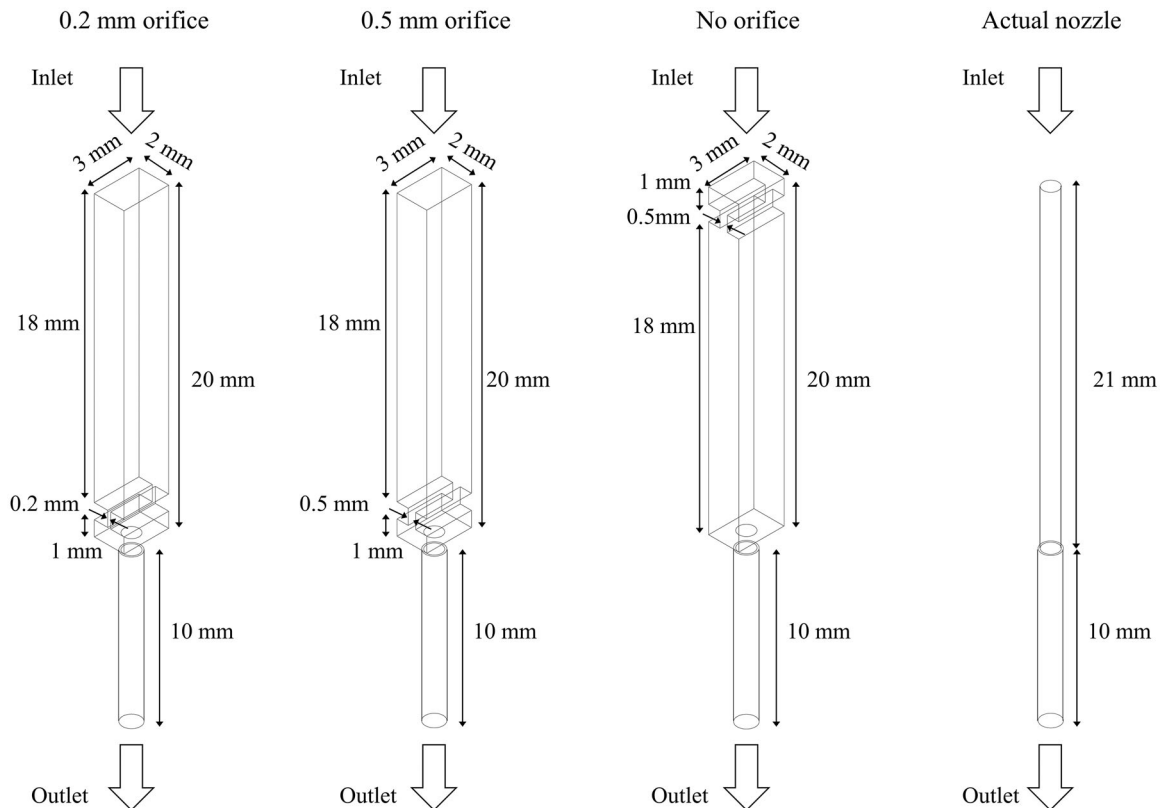

Figure 5. Schematic of the geometry for computational fluid dynamics (CFD) simulations for 4 cases of 0.2 mm orifice, 0.5 mm orifice, no orifice and actual nozzle.
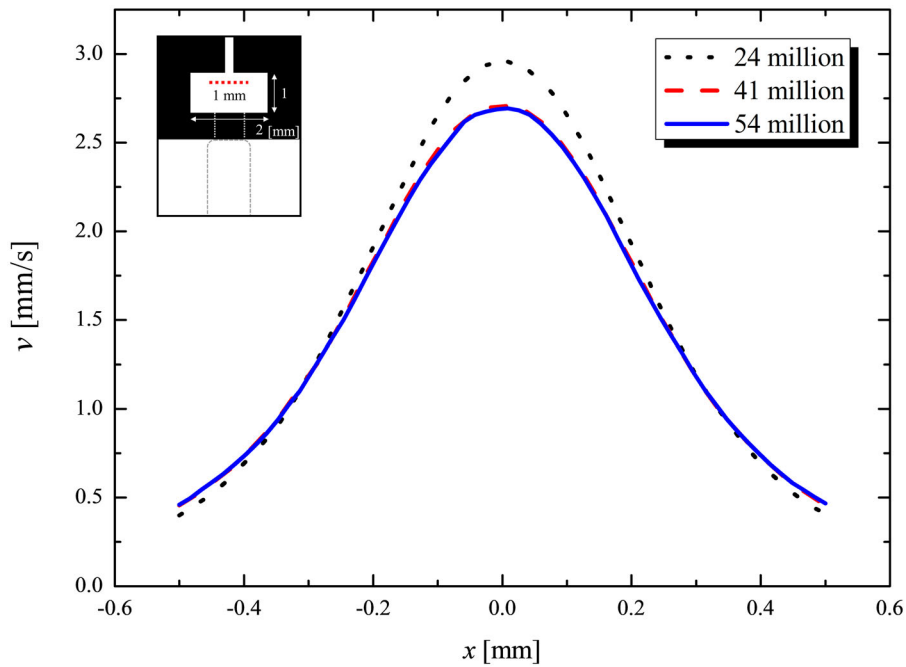
Figure 6. Comparison of velocity distribution at $y = 0.2$ mm downstream of the orifice in the flow direction. Plots are shown for three different number of mesh elements.

visualisation images on the inside of the nozzle flow channel. The images in Figure 8(a) from left to right correspond to 0.2 mm orifice, 0.5 mm orifice, no orifice and actual nozzle. Figure 8(b) shows images recorded after the nozzle exit in the same sequence. In the case of the nozzle flow channels including 0.2 and 0.5 mm orifices, as shown in Figure 8(a), the fibres are found to be aligned in a radial shape after passing through the orifice. However, in the case of no orifice and actual nozzle, the fibres were generally extruded parallel to the flow direction. Information such as the location and alignment angle of the clearly focused fibres was
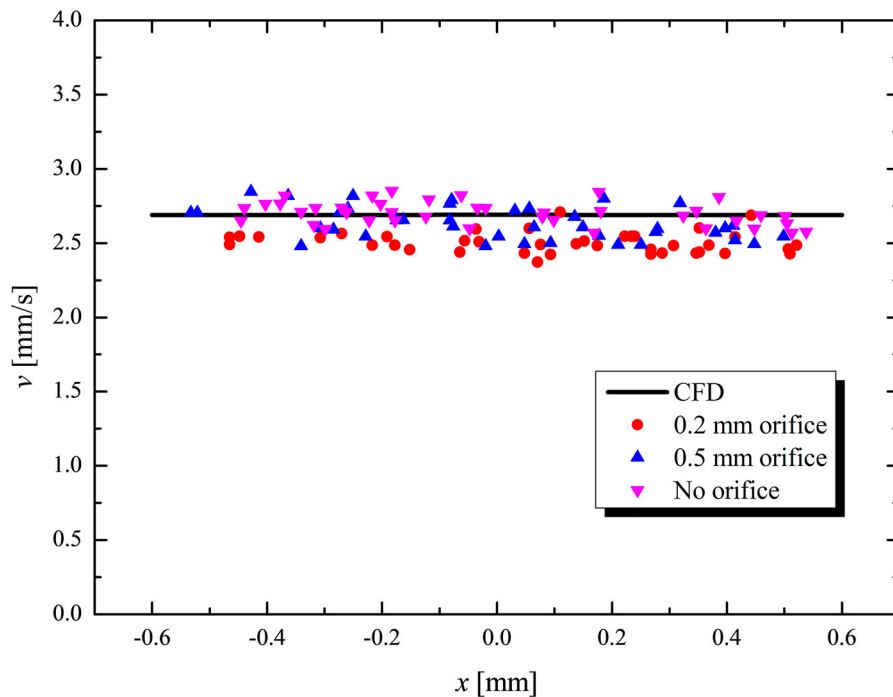

Figure 7. Comparison of extruder outlet velocity calculated by flow visualisation and CFD.
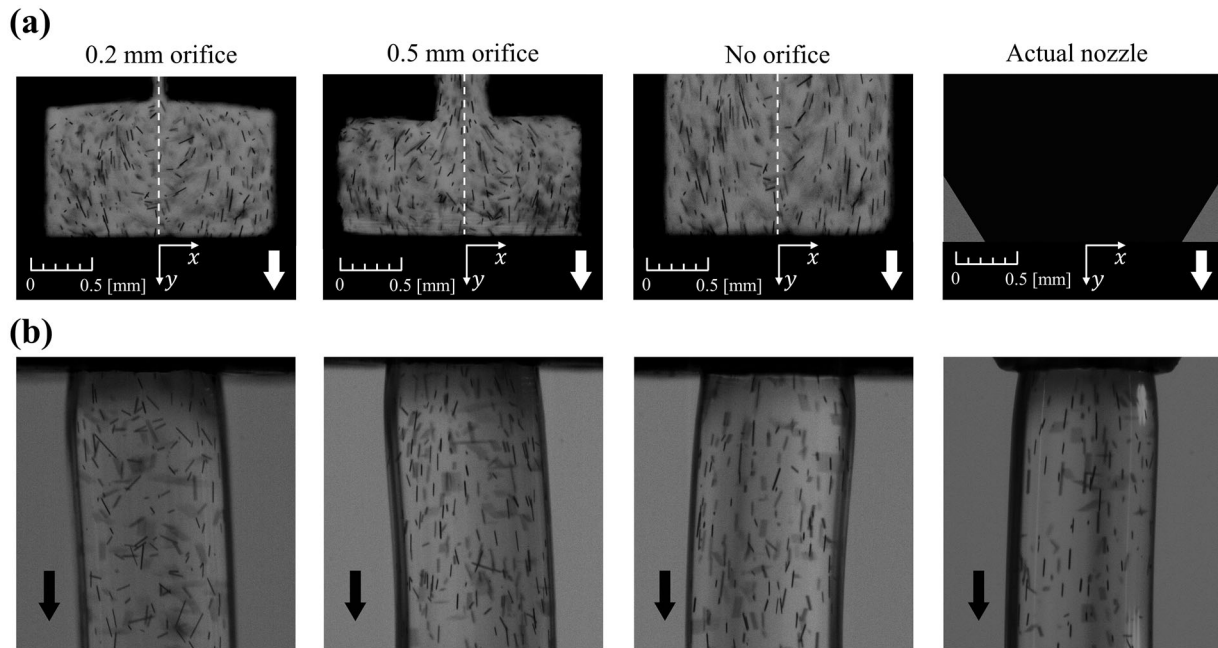
(a)

(b)

Figure 8. Images of the flow visualisation (a) inside and (b) outside of the extrusion nozzle, depending on the inner nozzle configuration for a flow rate of 0.2 mL/min.

obtained from these flow visualisation images by image processing.

As shown in Figure 9, filament extruded from the nozzle exhibited no significant change in the internal fibre alignment after bending to 90° on the bed until it hardens. Figure 9(a) shows flow visualisation images of the filament extruded from the nozzle with a 0.2 mm orifice flow channel to the bed and of the filament contacting the bed and bending to 90° after the nozzle

extrusion. To quantitatively analyse the fibre alignment change inside the filament after the nozzle extrusion, the average fibre angles in the 1 mm region towards the extruded filament progressing direction immediately after the nozzle exit (dotted line denoted as A in Figure 9(a)) and after being placed on the bed (dotted line denoted as A′ in Figure 9(a)) were calculated. For the fibre angle, a clockwise or a counterclockwise angle based on the filament progression direction is
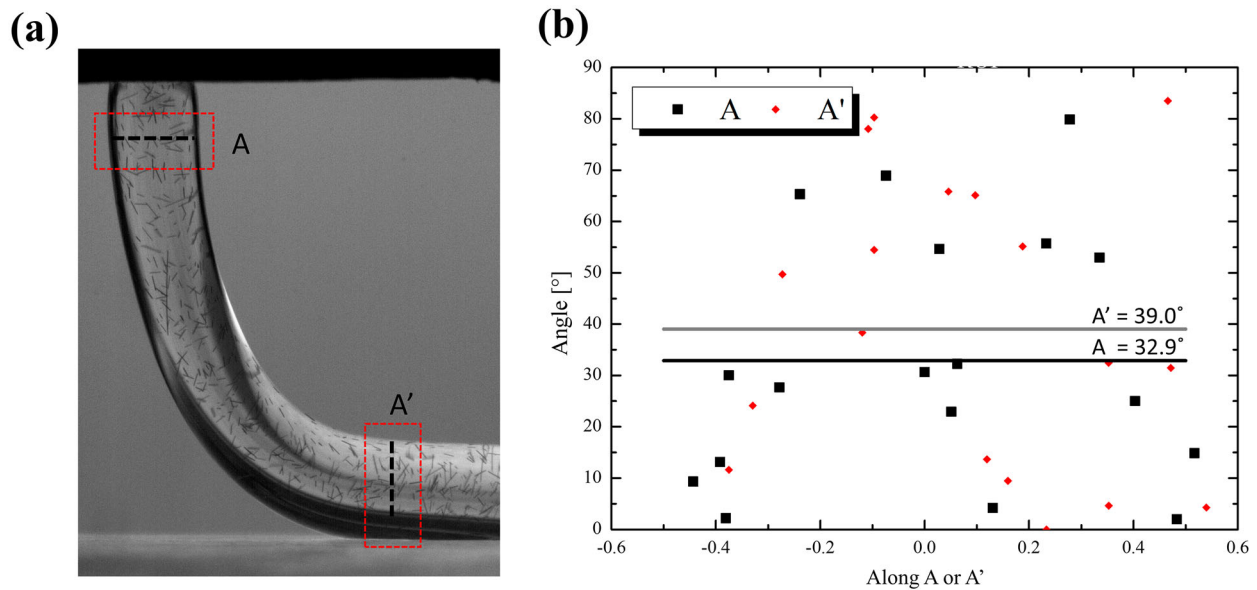
(a)

(b)

Figure 9. Comparison of alignment angle inside the extruded filament at the nozzle outlet and after deposited on the bed for 0.2 mm orifice for a flow rate of 0.2 mL/min: (a) flow visualisation image and (b) calculated alignment angles at lines A (nozzle outlet) and A′ (after bending 90° on the bed surface).

marked in Figure 9(b). The average values of 20 fibre angles calculated on A and A′ lines were 32.9° and 39.0°, respectively, showing a small difference. In particular, for the filament hardened on the bed, the fibre angle of the bottom part (touching the heating bed) accounting for 20% of the total length of A′ could not be included in the average value because of the shadow on the heating bed. The fibres inside the filament extruded from the nozzle are aligned more parallel to the flow direction near the edges contacting with air and the bed compared to those near the central part. Therefore, the fibre alignment angle at the nozzle extrusion exit and the bed surface were expected to be reduced more than the difference obtained from the aforementioned A and A′ lines. Although a single image was analysed in Figure 9, the analysis of additional images showed a very similar deviation in the average angle of fibre alignment between inside and outside the nozzle channel.

As determined from Figure 9, the fibre alignment value observed at the nozzle exit is similar to that hardened on the bed; hence, the flow visualisation experiments and the CFD analysis were limited to a ∼2 mm region of the flow channel inside the nozzle and after the extrusion. First, to compare the fibre alignment inside the nozzle and after the extrusion from the nozzle, by the flow visualisation, the fibre angles for different nozzles were calculated. Similar to the fibre angle shown in Figure 9, a clockwise or a counterclockwise angle is based on the filament progression direction (y-axis). The absolute value of the alignment angle is presented since the fibres show almost symmetrical alignment with respect to the vertical centre line in the flow direction. The alignment angle of fibres inside the nozzles at a flow rate of 0.2 mL/min is presented in

Figure 10. Figure 10 shows the scatter plot of the angles of a total of 24,000, 50,015, 25,067 and 4,651 fibres inside and outside the nozzles for the 0.2 mm orifice, 0.5 mm orifice, no orifice and actual nozzle flow channels, respectively. For the flow visualisation, experiments on the inside of the nozzle (Figure 10(a–c)), from the orifice to 1 mm downstream of the orifice, were selected as the object of observation. After the nozzle extrusion, the angles and locations of the fibres inside the 0–2 mm region in the filament length direction were calculated using the image processing method described in a previous section. Although the actual distance between the inside of the nozzle and the nozzle exit was longer than that marked in Figure 10, the flow visualisation results of the inside and outside of the nozzle, which were separately obtained, are schematised in Figure 10 for comparison.

Although it was observed that the fibre alignment angle at the nozzle exit and after deposited on the bed did not change, the additive alignment in the final FFF product may be different from what we see at the nozzle exit. This is because, as revealed in recent studies (Heller, Smith, and Jack 2019; Wang and Smith 2021; Consul et al. 2021), fibre alignment inside the extruded filaments may change additionally due to a squeeze flow between the nozzle and the bed or already deposited layer. The gap distance between the nozzle and the bed and the shape of free surface of the bead at the nozzle exit were found to affect the alignment of fibres inside the deposition and the resulting bulk mechanical properties. However, in this study, due to the emphasis on analysing the fibre alignment inside the nozzle channel, we have simplified the extruded filament to simply bend 90° on the bed. The impact of the squeeze flow on the final fibre alignment
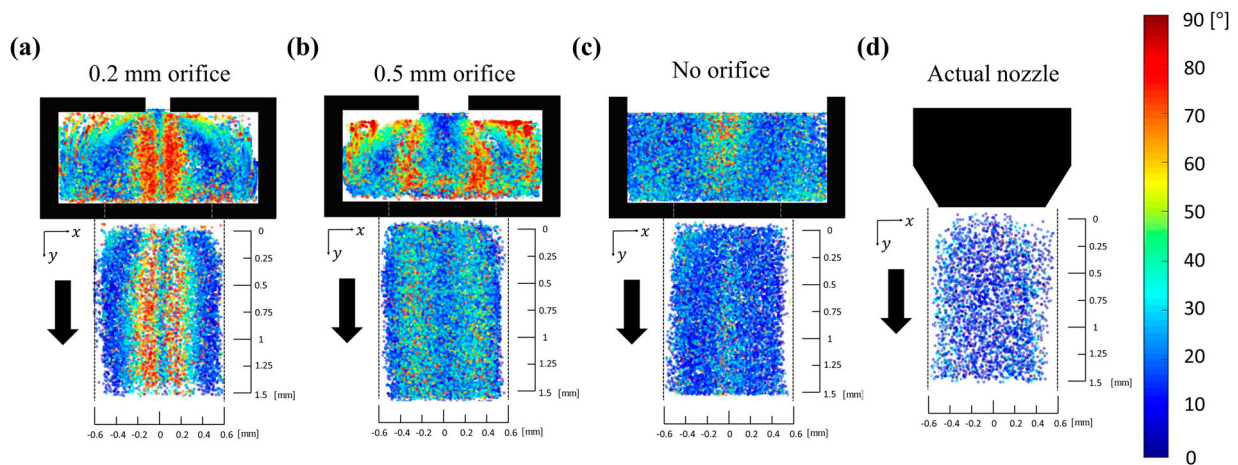

Figure 10. Scatter plot of alignment angle of fibres travelling inner and outer nozzle depending on inner nozzle configuration: (a) 0.2 mm orifice, (b) 0.5 mm orifice, (c) no orifice and (d) actual nozzle. Flow rate of the filament is fixed to 0.2 mL/min in all cases.

in the printed part may need further investigation, which may involve the optimisation of the printing process to obtain desired fibre alignment in the printed part.

From the fibre angle distribution in Figure 10, it is observed that more fibres with high angles marked in red and yellow are distributed around the filament centre part as the width of the orifice reduces. However, it was found that the fibres are generally aligned parallel to the filament heading direction in the filament edges and the whole region in the case of no orifice and orifice after the actual nozzle extrusion, respectively. The fibres extruded from the orifice did not show a clear alignment angle change before and after the nozzle extrusion. Moreover, in all experimental cases, it was observed that the fibres with a relatively higher angle at the periphery of the centre disperse to the periphery after being extruded from the nozzle. The maximum difference between the average angles inside the nozzle flow channel and after the extrusion is 6° for the 0.5 mm orifice case, indicating the aforementioned phenomenon. The fibres that pass through the orifice are parallel to the flow direction at the centreline, whereas the regions where the alignment angle rapidly increases are symmetrical to the centreline. For the 0.2 mm orifice case, the increase in the alignment angle was more rapid than that for the 0.5 mm orifice case. This trend is also found in Figure 11, which illustrates the average fibre angles in a 0–1.5 mm region after the nozzle exit for different filament flow rates. As previously observed in Figure 9, the fibre alignment angle does not change after the nozzle extrusion in all experiments.

Figure 11 presents results related to the fibre alignment angle immediately after the nozzle exit obtained with different filament flow rates and depending on the presence and thickness of the orifice. Although the filament extrusion speed was adjusted from 0.1 mL/min to 0.4 mL/min, the fibre alignment angles with different flow rates showed a negligible difference in all cases. Similar to a previous observation, the fibres with $|x| \leq 0.1$ mm based on centreline were aligned parallel to the extrusion direction in the nozzle with an orifice. However, when the fibres were out of this range, the fibre alignment rapidly became vertical to the flow direction. An *m*-shaped profile in which the decrease in fibre alignment angle towards the free surface was observed in the $|x| >= 0.2$ mm region. In contrast, in the no orifice nozzle case, the alignment angle of the centre part was slightly higher than that of the surrounding; however, no significant difference was found in general. Similarly, in the actual nozzle cases, the alignment angle of the left part was slightly higher than that of the right part; however, no large difference

occurred. One unexpected observation was that the fibre alignment angle was only dependent on the inside shape of the nozzle, and the flow velocity did not affect it. To gain a better understanding of the phenomenon that the fibre angle is not affected by the deep valley of the fibre angle and the flow rate at the filament centre found in the orifice-inserted nozzle, the flow visualisation results were compared with the shear and extension rates, which are the velocity gradients of the flow field calculated by the CFD analysis.

3.2. Comparison with shear rates

It was found that the speeds calculated by the CFD were in good agreement with those calculated by the flow visualisation experiments within a 3% error as shown in Figure 7. Moreover, it was found that the flow velocity at the centre, inside the filament, after the nozzle extrusion (*v*) and at the air interface does not show a large difference. The flow visualisation experimental results most similar to the CFD results were the case without an orifice and with a 0.5 mm orifice. However, in the case with a 0.2 mm orifice, the measured speed was 7% lower than the CFD speed. This was probably because in the 0.2 mm orifice test, slight leakage occurred between the assembled flow channel parts owing to the higher internal pressure than in other cases. To investigate the correlation between the fibre rotation and the gradient of the *x*-directional velocity components of the flow field inside the nozzle flow channel were analysed from the CFD result.

In the flow of a suspension including a fibre-type additive in the mould flow channel used in injection moulding, the flow direction gradient of velocity in the direction of flow, shear rate ($\partial v / \partial x$, $\dot{\gamma}$) and gradient of velocity perpendicular to the flow in the same direction, extension rate ($\partial u / \partial x$, $\dot{\varepsilon}$), are generally known to have the most significant effect on the fibre alignment. Furthermore, it is known that the shear rate arrays the fibres into the flow direction inside the mould flow channel, and the extension rate aligns in the direction vertical to the flow direction (Nguyen and Oh 2020; Trebbin et al. 2013). In this study, it is determined that the absolute size of these flow field gradients does not have a direct impact on the fibre alignment. This is because the shear and extension rates almost linearly increase with increasing flow velocity inside the nozzle flow channel. This can be seen in the CFD results of the nozzle with a 0.2 mm inserted orifice, and the calculation results of the 0.1 and 0.2 mL/min or 0.4 mL/min showed that the shear and extension rates increase exactly 2 and 4 times, respectively. However, Figure 11
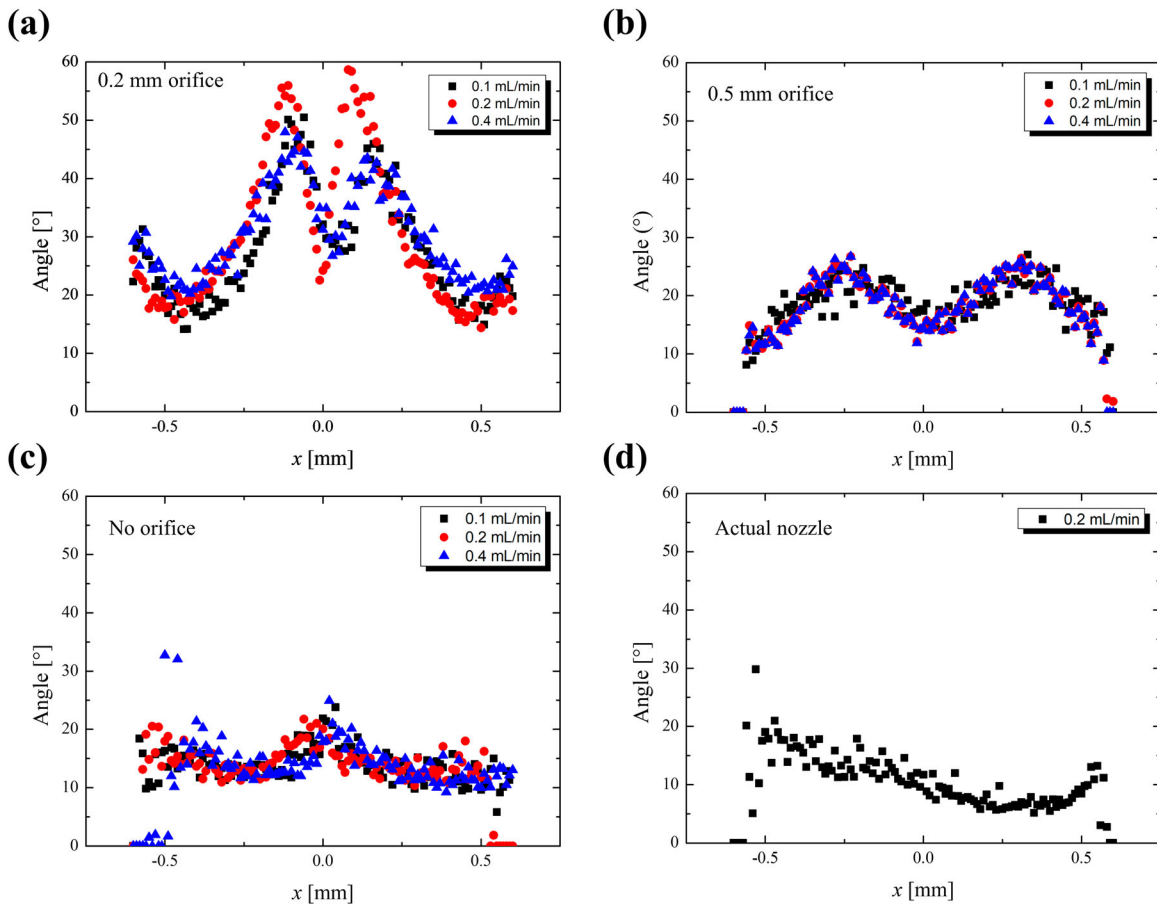
Figure 11. Averaged angle of fibres calculated at 0 mm ≤ y ≤ 1.5 mm where y = 0 is the nozzle outlet and y-axis represents the direction of filament extrusion. Angle of fibres is depicted along x-axis where x = 0 is the centre of the extruded filament depending on inner nozzle configuration having (a) 0.2 mm orifice, (b) 0.5 mm orifice, (c) no orifice and (d) actual nozzle.

also indicates that there is a negligible difference in these fibre alignment angle distributions. In this study, we assumed that the absolute value of the rate ratio $(\dot{\varepsilon}/|\dot{\gamma}|)$ between the extension and shear rates, a fibre alignment index proposed by Trebbin et al. (2013), affects the alignment inside the nozzle flow channel. Moreover, the absolute values of the rate ratios of the 0.2 mL/min case calculated using CFD are compared and presented in Figure 12. Fibre alignment in the direction vertical to the flow direction in the flow region with a rate ratio of over 0.14 was proposed in the flow visualisation research on the water suspension flow including cylindrical micelles in converging and diverging microchannels by X-ray (Trebbin et al. 2013).

Based on the comparison of the results shown in Figures 10 and 12, the rate ratio distribution inside the nozzle flow channel is calculated from CFD analysis. Moreover, the fibre alignment angles obtained from the flow visualisation experiments are generally similar. For the nozzles with 0.2- and 0.5-mm orifices, a high rate ratio and a large fibre alignment angle were obtained near the flow channel centreline, the orifice

outlet wall and the nozzle exit wall. It was also observed that the rate ratio and the fibre alignment angle at the wall of the nozzle exit are higher than those at the flow channel centre and other regions in the no orifice flow channel. For the nozzle with a 0.2 mm orifice, the rate ratio value of the red region is 75% higher than that of the 0.5 mm orifice case, which contributes to generally high fibre alignment angles. However, there are regions in which the rate ratio value and the fibre alignment angle do not follow a proportional relationship. For example, the high rate ratios in nozzles with an orifice were limited to the y ≤ 0.4 mm region at the orifice exit. However, a high fibre alignment angle at the centre was commonly found in the flow visualisation experiment even after the nozzle extrusion. This suggests that the rate ratio is not indirectly related to the fibre alignment angle but it involves the rotation of the fibres.

In a previous study explaining the vertical alignment of a fibre at the centre of the mould flow channel with an installed orifice (Nguyen and Oh 2020), it was concluded that a high extension rate or rate ratio results in a high
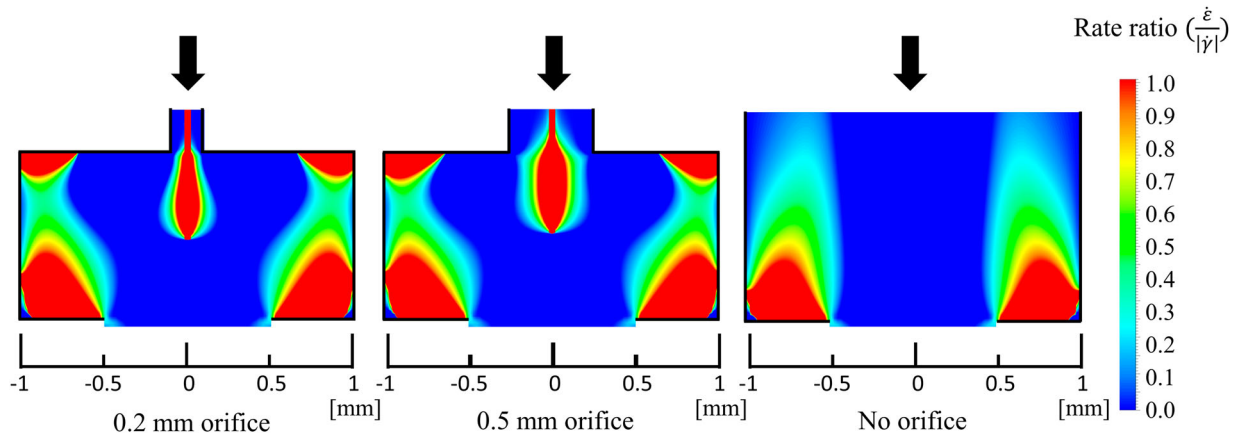
Figure 12. CFD calculation of rate ratio depending on the nozzle channel configuration for a flow rate of 0.2 mL/min.

correlation with the rotating moment of the fibre. Moreover, the aforementioned phenomenon can be explained using this analysis. Therefore, because of the high rate ratio in the $y \leq 0.4$ mm region at the centre, the fibres rotate and align in the direction vertical to the flow direction. After passing through this region, the fibres gradually align back to the flow direction owing to the relatively low rate ratio. If the nozzle path flow is long, it is expected that the vertically aligned fibres will ultimately recover the parallel alignment to the flow direction because of the extension rate being close to zero and the low shear rate that is relatively higher than the extension rate. However, in the nozzle of this experiment, the fibre is extruded to the nozzle exit after passing through the orifice and subsequently the 1 mm flow channel, following which it is additionally aligned at the nozzle exit. Moreover, after the nozzle extrusion, the shear or extension rate converges to zero. Therefore, there is no change in the fibre alignment after deposited on the bed, similar to in the flow channel inside the nozzle.

A similar discussion can be made when predicting the fibre alignment of different viscosity of the working fluid. In an actual FFF process, the viscosity of polymer melts is at least an order of magnitude higher compared to the working fluid in this study. We believe that this viscosity difference does not impact the relative flow field inside or outside the nozzle. The difference in viscosity may impact the extension and share rates in the flow, but not the rate ratio, which is the key parameter that governs fibre alignment. This is supported by simulations that show a negligible change in rate ratio with the fluid viscosity. Furthermore, in separate experiments to investigate this further, fibre alignment inside the nozzle channel with 0.2 mm orifice with base PDMS of Sylgard 184 and Sylgard 186 showed a negligible difference in alignment angle inside the nozzle flow despite a

20× difference in the viscosity of the two polymers. Based on such comparison, we believe the fibre alignments in the actual FFF process with higher viscosity are likely to be similar to the current fibre alignment.

3.3. Discussion on parallel alignment in the nozzle centre

The part not investigated by the analysis of the correlation between the shear and extension rate ratio and the fibre alignment inside the nozzle flow channel is the fibre alignment at the centre of the flow channel observed in the flow visualisation experiments including an orifice flow channel. The phenomenon that the fibre alignment profile has a valley shape in the $|x| \leq 0.2$ mm region, as shown in Figures 10 and 11, is unusual and conflicts with the previous flow visualisation experimental results in the injection mould flow channel passing through an orifice (Nguyen and Oh 2020). Based on the rate ratio calculated by CFD, it was also determined that the rate ratio at the centre is higher than in regions where fibre alignment angles have a higher value. In Figure 13(a), the flow visualisation results imitating the mould flow channel for the same shaped orifice and the expansion channel elongated to 20 mm are compared with those of the nozzle path flow including a 0.2 mm orifice. In general, the fibres that passed through the orifice were dispersed in a radial-shaped alignment centring around the centre of the flow channel. However, in terms of the flow channel inside the nozzle, fibres flowing close to the centreline were found to be parallelly aligned. The comparison results of the rate ratio calculated by the CFD analysis of the injection mould and nozzle flow channels are presented in Figure 13 (b). Generally, similar profiles were observed, except
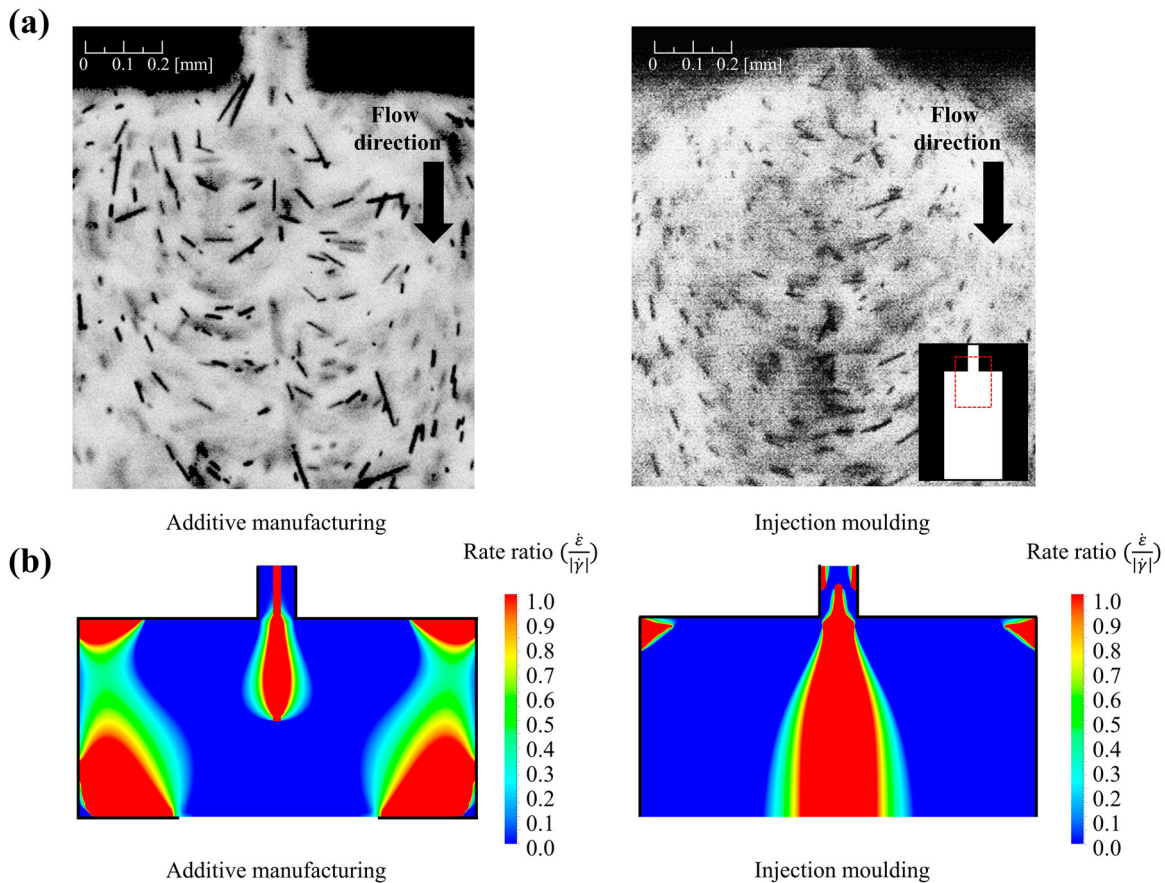
(a)

(b)

Figure 13. Comparison of fibre alignment in 0.2 mm orifice nozzle and injection moulding channel 0.2 mm orifice, (a) flow visualisation images and (b) rate ratio calculated by CFD.

that the rate ratio was related to the downstream of the flow channel in the mould flow channel.

To observe the parallel alignment of fibres at the centre of the nozzle channel including an orifice in detail, Figure 14 shows the sequential flow visualisation images over time for the zoomed-in region of the 0.2 mm orifice exit. It is shown that all fibres recorded with a 0.05 s time interval move in the PDMS medium with a flow speed of 0.2 mL/min. The bottom part in Figure 14 shows the reconstruction of the location and angle changes of the five representative fibres marked in red dotted ovals. First, it was found that the fibres flowing close to the flow channel wall after exiting the orifice (two fibres near $x = -0.25$ and 0.3 mm) were aligned in a vertical direction of the fibre alignment, as they moved towards walls. However, they rapidly recovered the alignment in the flow direction. In contrast, the fibres located at $x = \pm 0.08$ mm were rapidly aligned in a vertical direction when exiting the orifice, and this alignment was maintained. Finally, the fibres flowing close to the flow channel centreline ($x = 0.04$ mm) were aligned parallel to the flow direction from the orifice exit, and the

fibre angle did not change. This is clearly a different alignment phenomenon from those of the fibres at the centre of the flow channel that passed through the orifice inside the injection mould, as shown in Figure 13. This phenomenon occurred in several repetitive experiments and was observed regardless of the flow channel orientation to the gravity, flow speed and orifice spacing. Until now, this phenomenon is found in a nozzle flow channel with a distance of less than 3 mm between the orifice and the extrusion nozzle. It is a new alignment phenomenon not observed inside an internal flow channel as in an injection mould. The reason behind this observation will be revealed in future experiments on various flow channel shapes and CFD analysis accounting viscoelastic effects of composite mixture.

Flow visualisation and CFD analyses described above indicate that more carbon fibres inside the filament extruded through an orifice-included nozzle are aligned in through-plane than through the nozzle without an orifice. Finally, Figure 15 presents the fibre angle in an approximately 2 mm region to the y-direction after the nozzle extrusion at a flow speed of 0.2
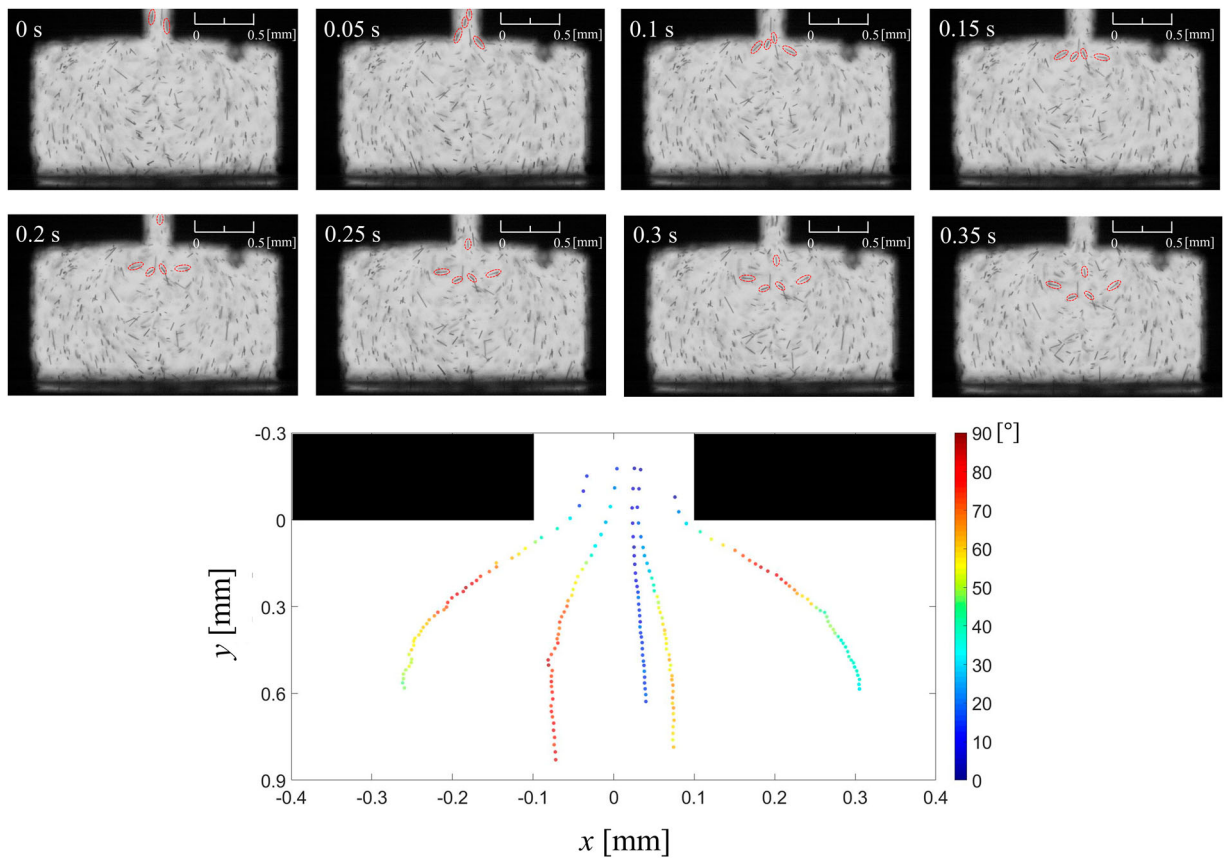
Figure 14. Sequential images of flow visualisation of fibre alignment inside nozzle channel with 0.2 mm orifice for a flow rate of 0.2 mL/min (top) and a reconstructed image showing the evolution of alignment of 5 representative fibres travelling channel centre and surrounding regions (bottom).

mL/min for all nozzle cases. The angle marked here is the value obtained by averaging all fibre angles calculated for the $|x| \leq 0.6$ mm region in the y range of the 0.01 mm interval. It was again found that the fibre alignment angle change is negligible after the extrusion. Moreover, it was observed that the nozzle including an orifice with a smaller width shows an increase in the vertical alignment of the fibre. With the 0.2 mm orifice nozzle, the angles of all extruded fibres were 26.5°, which is a distinctly higher alignment angle than that of the 0.5 mm orifice nozzle (19.2°), no orifice nozzle (15.2°) and actual nozzle (11.6°). These results experimentally determined that the fibres can be aligned in a vertical direction in the flow profile through a structure in which the flow channel width inside the nozzle contracts and expands.

It is important to recognise key limitations and assumptions underlying the present work. Only a limited number of nozzle designs have been used in this work, mainly based on enabling good quality flow visualisation. These nozzle designs are not necessarily optimal from fibre alignment perspective, but certainly help provide the fundamental knowledge of fibre

alignments of the interior and exterior of the FFF nozzle. The flow after the nozzle exit is simplified which does not account for a squeezing effect between the nozzle exit and the bed. Due to such simplification, fibre alignment inside the extruded filament reported here may contain some uncertainty compared to an actual FFF process with a narrower gap height between the nozzle exit and the bed.

Based on the key findings reported here, a number of directions for future work are recommended. Multiphase simulations that predict fibre alignment in detail may be helpful in further understanding the mechanics of fibre-polymer composite. Printing with longer and high-volume fibres, with alignment control using techniques similar to those described here, may be very beneficial. Nevertheless, the comparison of the flow field inside the nozzle and the flow visualisation experiment in the present study would broaden the understanding of the alignment of additives in the FFF process and may enable the design of 3D printing nozzles with controlled additive alignment angle inside the printed product. Additionally, it will enable FFF products with higher thermal properties in the through-plane and layer-layer
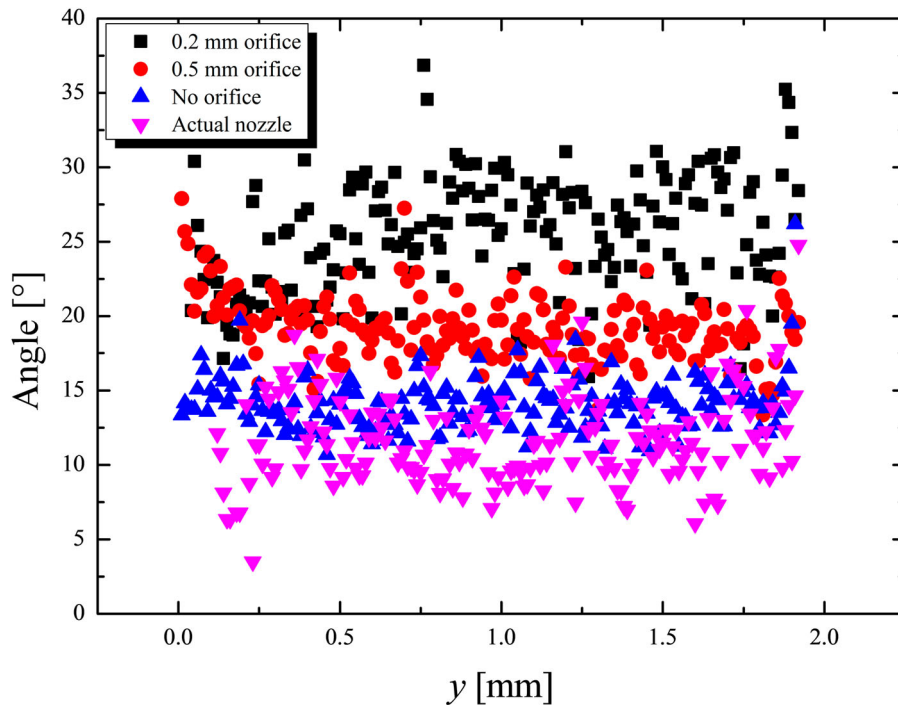
Figure 15. Average alignment angle of fibres along the extrusion direction after the filament is extruded from the nozzle for different nozzle configurations at a flow rate of 0.2 mL/min.

direction which were not possible with conventional nozzles and other techniques such as raster sequencing.

4. Conclusions

Polymer-fibre composites present a promising technique for improving the mechanical and thermal properties of 3D printed parts. However, fibre alignment in filaments is critical to achieve the desired enhancement and to maximise the benefit of the composite properties within a small fibre fraction. Both experimental and simulation aspects of this work contribute towards these goals. The FFF process using a polymer composite containing carbon fibres was simulated with an orifice installed inside the nozzle channel, and the corresponding fibre alignment was observed by flow visualisation experiments. A nozzle with a 0.2 mm orifice showed a larger fibre alignment angle than a 0.5 mm orifice nozzle, a no orifice nozzle and an actual nozzle channels. It was found that the fibre alignment is not affected by the filament flow rate and is highly correlated with the rate ratio, an absolute ratio of the extension and shear rates in the nozzle flow channel, obtained from CFD analysis.

However, the parallel alignment phenomenon of the fibre that locally occurs at the centre of the flow channel of a nozzle with an installed orifice is irrelevant to the rate ratio. This is a new phenomenon that did not occur in the existing flow visualisation experiments conducted inside an injection mould with the same orifice channel. To investigate the physical reasons for this phenomenon, future flow visualisation tests on various forms of orifices and nozzle flow channels may be required. These insights from this work may help design FFF materials and processes that lead to better fibre alignment and improved high through-layer physical properties. Potential applications include printing of high thermal conductivity for advanced thermal systems, multi-functional parts for bio-applications and multi-layered 3D electronics.

Disclosure statement

No potential conflict of interest was reported by the author(s).

Notes on contributors

Do-In Jeong is currently pursuing Master's degree at the Department of Mechanical Engineering at Chosun University, Korea. His research interests include understanding the alignment of additives inside polymer medium during the additive manufacturing process.

Ankur Jain is an Associate Professor in the Mechanical and Aerospace Engineering Department at the University of Texas at Arlington. He has published 96 journal papers on topics related to theoretical and applied heat transfer, including in additive manufacturing, batteries and microelectronics. He is a recipient of the NSF CAREER Award in 2016, UT

Arlington College of Engineering Outstanding Early Career Award in 2017 and Lockheed Martin Aeronautics Excellence in Teaching Award in 2018. He received his Ph.D. from Stanford University in 2007.

Dong-Wook Oh is an Associate Professor in the Department of Mechanical Engineering at Chosun University, Korea.   He received his Ph.D. from Seoul National University in 2008. Prior to joining Chosun University, he worked as a Senior Researcher at the Department of Extreme Thermal Systems, Korea Institute of Machinery and Materials and a Post-Doctoral Associate at the Department of Material Science and Engineering, University of Illinois at Urbana-Champaign. His current research is focused on thermal characterisation and application of polymer composites.

ORCID

Ankur Jain 🔵 http://orcid.org/0000-0001-5573-0674
Dong-Wook Oh 🔵 http://orcid.org/0000-0003-1626-6930

References

Anwer, A., and H. E. Naguib. 2018. "Multi-Functional Flexible Carbon Fiber Composites with Controlled Fiber Alignment Using Additive Manufacturing." *Additive Manufacturing* 22: 360–367.

Berretta, S., R. Davies, Y. T. Shyng, Y. Wang, and O. Ghita. 2017. "Fused Deposition Modelling of High Temperature Polymers: Exploring CNT PEEK Composites." *Polymer Testing* 63: 251–262.

Butler, P. 1999. "Shear Induced Structures and Transformations in Complex Fluids." *Current Opinion in Colloid & Interface Science* 4 (3): 214–221.

Caminero, M. A., J. M. Chacón, I. García-Moreno, and G. P. Rodríguez. 2018. "Impact Damage Resistance of 3D Printed Continuous Fibre Reinforced Thermoplastic Composites Using Fused Deposition Modelling." *Composites Part B: Engineering* 148: 93–103.

Castles, F., D. Isakov, A. Lui, Q. Lei, C. E. Dancer, Y. Wang, J. M. Janurudin, S. C. Speller, C. R. Grovenor, and P. S. Grant. 2016. "Microwave Dielectric Characterisation of 3D-Printed BaTiO$_3$/ABS Polymer Composites." *Scientific Reports* 6: 22714.

Chen, L., Y. Wu, and L. Jiang. 2019. "Recent Advances in One-Dimensional Assembly of Nanoparticles." *Chemical Society Reviews* 48 (1): 8–21.

Consul, P., K. U. Beuerlein, G. Luzha, and K. Drechsler. 2021. "Effect of Extrusion Parameters on Short Fiber Alignment in Fused Filament Fabrication." *Polymers* 13 (15): 2443.

El Moumen, A., M. Tarfaoui, and K. Lafdi. 2019. "Additive Manufacturing of Polymer Composites: Processing and Modeling Approaches." *Composites Part B: Engineering* 171: 166–182.

Gardner, J. M., G. Sauti, J. W. Kim, R. J. Cano, R. A. Wincheski, C. J. Stelter, B. W. Grimsley, D. C. Working, and E. J. Siochia. 2016. "3-D Printing of Multifunctional Carbon Nanotube Yarn Reinforced Components." *Additive Manufacturing* 12: 38–44.

Goh, G. L., S. Agarwala, and W. Y. Yeong. 2019. "Directed and On-Demand Alignment of Carbon Nanotube: A Review Toward 3D Printing of Electronics." *Advanced Materials Interfaces* 6: 1801318.

Goh, G. D., and W. Y. Yeong. 2018. "Mode I Interlaminar Fracture Toughness of Additively Manufactured Carbon Fibre Thermoplastic." Proceedings of the 3rd international conference on progress in additive manufacturing, 505–510.

Goh, G. L., H. Zhang, T. H. Chong, and W. Y. Yeong. 2021. "3D Printing of Multilayered and Multimaterial Electronics: A Review." *Advanced Electronic Materials* 2100445.

Gong, S., Z. H. Zhu, and S. A. Meguid. 2015. "Anisotropic Electrical Conductivity of Polymer Composites with Aligned Carbon Nanotubes." *Polymer* 56: 498–506.

Guo, S. Z., X. Yang, M. C. Heuzey, and D. Therriault. 2015. "3D Printing of a Multifunctional Nanocomposite Helical Liquid Sensor." *Nanoscale* 7 (15): 6451–6456.

Heller, B. P., D. E. Smith, and D. A. Jack. 2019. "Planar Deposition Flow Modeling of Fiber Filled Composites in Large Area Additive Manufacturing." *Additive Manufacturing* 25: 227–238.

Holmes, L. R., and J. C. Riddick. 2014. "Research Summary of an Additive Manufacturing Technology for the Fabrication of 3D Composites with Tailored Internal Structure." *JOM* 66 (2): 270–274.

Hwang, S., E. I. Reyes, K.-S. Moon, R. C. Rumpf, and N. S. Kim. 2014. "Thermo-mechanical Characterization of Metal/Polymer Composite Filaments and Printing Parameter Study for Fused Deposition Modeling in the 3D Printing Process." *Journal of Electronic Materials* 44 (3): 771–777.

Kausar, A. 2019. "Review on Conducting Polymer/Nanodiamond Nanocomposites: Essences and Functional Performance." *Journal of Plastic Film & Sheeting* 35 (4): 331–353.

Kennedy, P., and R. Zheng. 2013. *Flow Analysis of Injection Molds*, 2nd ed. Munchen: Carl Hanser Verlag GmbH & Co. KG.

Kokkinis, D., M. Schaffner, and A. R. Studart. 2015. "Multimaterial Magnetically Assisted 3D Printing of Composite Materials." *Nature Communications* 6: 8643.

Lewicki, S. 2018. "Additive Manufacturing of Short and Mixed Fibre-Reinforced Polymer." U.S. Patent 20170015061A1.

Lewis, J. A. 2006. "Direct ink Writing of 3D Functional Materials." *Advanced Functional Materials* 16: 2193–2204.

Mohan, N., P. Senthil, S. Vinodh, and N. Jayanth. 2017. "A Review on Composite Materials and Process Parameters Optimisation for the Fused Deposition Modelling Process." *Virtual and Physical Prototyping* 12: 47–59.

Mulholland, T., S. Goris, J. Boxleitner, T. A. Osswald, and N. Rudolph. 2018. "Process-Induced Fiber Orientation in Fused Filament Fabrication." *Journal of Composites Science* 2 (3): 45.

Nagarajan, B., A. F. Eufracio Aguilera, M. Wiechmann, A. J. Qureshi, and P. Mertiny. 2018. "Characterization of Magnetic Particle Alignment in Photosensitive Polymer Resin: A Preliminary Study for Additive Manufacturing Processes." *Additive Manufacturing* 22: 528–536.

Nguyen, H. M. K., and D.-W. Oh. 2020. "Analysis of Carbon Fiber Alignment in a Polydimethylsiloxane Matrix Flowing in an Orifice Channel." *Journal of Molecular Liquids* 317: 113978.

Nikzad, M., S. H. Masood, and I. Sbarski. 2011. "Thermo-mechanical Properties of a Highly Filled Polymeric Composites for Fused Deposition Modeling." *Materials & Design* 32 (6): 3448–3456.

Ning, F., W. Cong, J. Qiu, J. Wei, and S. Wang. 2015. "Additive Manufacturing of Carbon Fiber Reinforced Thermoplastic Composites Using Fused Deposition Modeling." *Composites Part B: Engineering* 80: 369–378.

Ozbolat, V., M. Dey, B. Ayan, A. Povilianskas, M. C. Demirel, and I. T. Ozbolat. 2018. "3D Printing of PDMS Improves its Mechanical and Cell Adhesion Properties." *ACS Biomaterials Science & Engineering* 4 (2): 682–693.

Pathanasiou, T. D., and D. C. Guell. 1997. *Flow-induced Alignment in Composite Materials*. Sawston: Woodh. Publ.

Prajapati, H., D. Ravoori, R. L. Woods, and A. Jain. 2018. "Measurement of Anisotropic Thermal Conductivity and Inter-Layer Thermal Contact Resistance in Polymer Fused Deposition Modeling (FDM)." *Additive Manufacturing* 21: 84–90.

Shofner, M., K. Lozano, F. Rodríguez-Macías, and E. Barrera. 2003. "Nanofiber-Reinforced Polymers Prepared by Fused Deposition Modeling." *Journal of Applied Polymer Science* 89 (11): 3081–3090.

Shulga, E., R. Karamov, I. S. Sergeichev, S. D. Konev, L. I. Shurygina, I. S. Akhatov, S. D. Shandakov, and A. G. Nasibulin. 2020. "Fused Filament Fabricated Polypropylene Composite Reinforced by Aligned Glass Fibers." *Materials* 13 (16): 3442.

Su, S.-H., Y. Huang, S. Qu, W. Liu, R. Liu, and L. Li. 2018. "Microdiamond/PLA Composites with Enhanced Thermal Conductivity Through Improving Filler/Matrix Interface Compatibility." *Diamond and Related Materials* 81: 161–167.

Su, B., Y. Wu, and L. Jiang. 2012. "The Art of Aligning one-Dimensional (1D) Nanostructures." *Chemical Society Reviews* 41 (23): 7832–7856.

Sylgard 186 Silicone Elastomer Technical Data Sheet, Dow Co. www.dow.com/content/dam/dcc/documents/en-us/productdatasheet/11/11-12/11-1253-sylgard-186-silicone-elastomer.pdf.

Tekinalp, H. L., V. Kunc, G. M. Velez-Garcia, C. E. Duty, L. J. Love, A. K. Naskar, C. A. Blue, and S. Ozcan. 2014. "Highly Oriented Carbon Fiber–Polymer Composites via Additive Manufacturing." *Composites Science and Technology* 105: 144–150.

Trebbin, M., D. Steinhauser, J. Perlich, A. Buffet, S. V. Roth, W. Zimmermann, J. Thiele, and S. Forster. 2013. "Anisotropic Particles Align Perpendicular to the Flow Direction in Narrow Microchannels." *Proceedings of the National Academy of Sciences* 110 (17): 6706–6711.

Waheed, S., J. M. Cabot, P. Smejkal, S. Farajikhah, S. Sayyar, P. C. Innis, S. Beirne, et al. 2019. "Three-Dimensional Printing of Abrasive, Hard, and Thermally Conductive Synthetic Microdiamond-Polymer Composite Using Low-Cost Fused Deposition Modeling Printer." *ACS Applied Materials & Interfaces* 11 (4): 4353–4363.

Wang, Z., and D. E. Smith. 2021. "A Fully Coupled Simulation of Planar Deposition Flow and Fiber Orientation in Polymer Composites Additive Manufacturing." *Materials* 14 (10): 2596.

Yan, H., Y. Tang, W. Long, and Y. Li. 2014. "Enhanced Thermal Conductivity in Polymer Composites with Aligned Graphene Nanosheets." *Journal of Materials Science* 49 (15): 5256–5264.

Yeong, W. Y., and G. D. Goh. 2020. "3D Printing of Carbon Fiber Composite: The Future of Composite Industry?" *Matter* 2 (6): 1361–1363.

Young, D., N. Wetmore, and M. Czabaj. 2018. "Interlayer Fracture Toughness of Additively Manufactured Unreinforced and Carbon-Fiber-Reinforced Acrylonitrile Butadiene Styrene." *Additive Manufacturing* 22: 508–515.

Yuan, C., B. Duan, L. Li, B. Xie, M. Huang, and X. Luo. 2015. "Thermal Conductivity of Polymer-Based Composites with Magnetic Aligned Hexagonal Boron Nitride Platelets." *ACS Applied Materials & Interfaces* 7 (23): 13000–6.

Yuan, S., F. Shen, C. K. Chua, and K. Zhou. 2019. "Polymeric Composites for Powder-Based Additive Manufacturing: Materials and Applications." *Progress in Polymer Science* 91: 141–168.